SCIPEDIA

Modeling and Simulation of a Novel Permanent Magnet Motor for Enhanced Vehicle Steering Performance

Mahmud Ebrahim Assen* and Guoqing Geng

Vehicle Engineering, School of Automotive and Traffic Engineering, Jiangsu University, Zhenjiang, 212013, China

INFORMATION

Keywords:
Magnetic flux
permanent magnet motor (PMM)
torque density
torque ripple
steering by wire

DOI: 10.23967/j.rimni.2025.10.74195

SCIPEDIA Revista Internacional de Métodos Numéricos para Cálculo y Diseño en Ingeniería

Revista Internacional Métodos numéricos para cálculo y diseño en ingeniería RIMNI in cooperation with CIMNE

Modeling and Simulation of a Novel Permanent Magnet Motor for Enhanced Vehicle Steering Performance

Mahmud Ebrahim Assen* **and Guoqing Geng**

Vehicle Engineering, School of Automotive and Traffic Engineering, Jiangsu University, Zhenjiang, 212013, China

ABSTRACT

This paper introduces a new design for a permanent magnet motor (PMM) tailored for automotive steering applications. By utilizing new permanent magnet topology, high-performance materials, and rotor designs, the newly proposed PMM design reduces torque ripple while boosting torque density. This design is integrated within a sophisticated steer-by-wire (SBW) system, enabling seamless operation and reliable feedback, which are crucial for modern vehicles. The finite element analysis (FEA) substantiates the effectiveness of the proposed PMM, resulting in a 1.2% enhancement in magnetic flux density, a 4.65% increase in static torque, and a 4.4% reduction in torque ripple. This research addresses the issues in wheel steering technology and lays the groundwork for future automotive motor technologies. And also, it provides valuable insights into the development of automotive technologies, paving the way for enhanced performance and sustainability in the automotive sector. Furthermore, these improvements not only aim to enhance driver satisfaction but also align with the industry's transition toward greener technologies.

OPEN ACCESS

Received: 05/10/2025

Accepted: 15/12/2025

DOI
10.23967/j.rimni.2025.10.74195

Keywords:
Magnetic flux
permanent magnet motor (PMM)
torque density
torque ripple
steering by wire

1 Introduction

Recent advancements in the automotive industry have initiated a shift from traditional mechanical systems to modern electronic solutions. Over the past century, vehicle steering systems have evolved from purely mechanical linkages to sophisticated electronically controlled designs [1]. Current research and development efforts focus on enhancing vehicle dynamics, safety, and energy efficiency by integrating advanced motor technologies [2,3]. Historically, hydraulic power steering (HPS) systems have been the norm [4]; however, recent trends suggest a notable paradigm shift toward high-bandwidth, energy-efficient systems that utilize permanent magnet synchronous motors (PMSM) [5–8].

The increasing adoption of permanent magnet synchronous motor (PMSM)-based wheel steering is primarily driven by their advantages in overcoming the limitations of traditional systems. Unlike HPS, PMSM provides superior control resolution, enabling direct and independent torque vectoring at individual wheel hubs. This granular control supports the implementation of active steering systems that dynamically adjust steering angles based on real-time kinematic and dynamic vehicle states, alongside sophisticated torque vectoring strategies that enhance cornering stability and agility [9].

*Correspondence: Mahmud Ebrahim Assen. (5102230323@stmail.ujs.edu.cn).

The resulting improvements in vehicle handling and dynamic response directly correlate to heightened driver safety and performance, especially in adverse driving conditions in various applications [10,11].

Moreover, the elimination of complex hydraulic circuits leads to reduced vehicle mass, minimized energy consumption, and streamlined maintenance requirements, aligning with the growing demand for sustainable automotive solutions. Beyond immediate performance enhancements, PMSM-based steering systems have the potential to redefine vehicle design and functionality. Their compact form factor and flexible integration capabilities encourage re-evaluation of wheel hub designs, facilitating innovative steering geometries and optimized suspension kinematics [12–16]. Additionally, the high-resolution feedback signals provided by PMSM enable the development of advanced control algorithms capable of adapting to varying road surfaces, driver inputs, and environmental conditions. As research and development in this field accelerates, PMSM-driven wheel steering is set to become a foundational technology in the next generation of vehicles, promising a driving experience characterized by enhanced safety, increased engagement, and reduced environmental impact [8,9,17,18].

Despite these advances, basic arc-shaped PM designs often encounter issues related to structural integrity and magnetic performance. This study introduces a new L-shaped PM design that enhances mechanical strength and magnetic flux distribution, resulting in better torque. This study presents an innovative design of a permanent magnet synchronous motor (PMSM), as depicted in Fig. 1 and the simplified model in Fig. 2. The rotor (1) is the rotating component in electric machines, interacting with the stationary stator (3), which contains windings that generate a magnetic field. Innovations like the new permanent magnet topology (2) optimize magnet arrangements to enhance efficiency and performance. Windings (4), made of coils of wire, play a crucial role in producing the magnetic fields necessary for the machine's operation, ultimately contributing to torque generation and overall performance. The organization of the study is as follows: Section 2 outlines the materials and methods used; Section 3 discusses the numerical analysis conducted; Section 4 presents the results and includes discussions, along with model validation through comparisons with established models. Finally, the study concludes by offering insights and recommendations for future research.

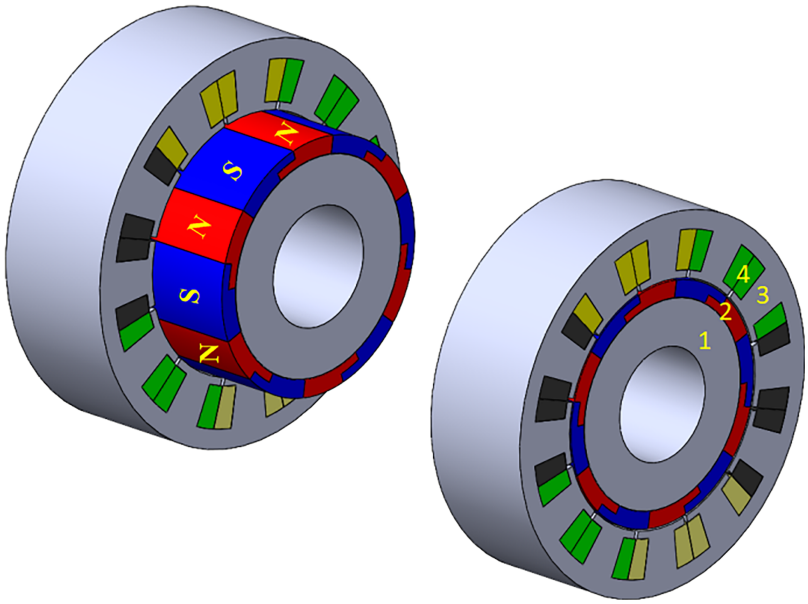

Figure 1: The proposed new 3D model of PMSM

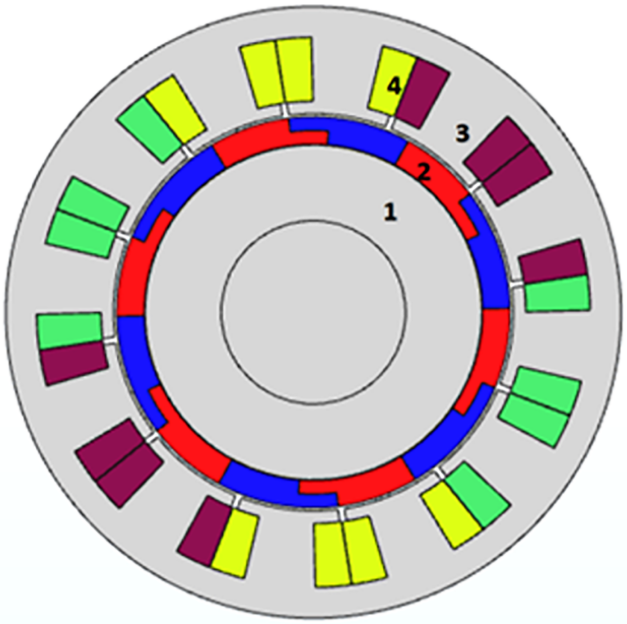

Figure 2: The simplified 2D mode of new PMSM. 1: rotor, 2: new permanent magnet topology, 3: stator, 4: winding

2 Material and Method

Mathematical analysis and modeling are essential for understanding how different factors affect system performance (see Fig. 3). This section provides the mathematical formulations for modeling the permanent magnet synchronous motor (PMSM), based on key assumptions: the permanent magnets are surface-mounted and radially magnetized. It also assumes that the ferromagnetic core material follows a linear B-H curve and that magnetic saturation effects can be disregarded.

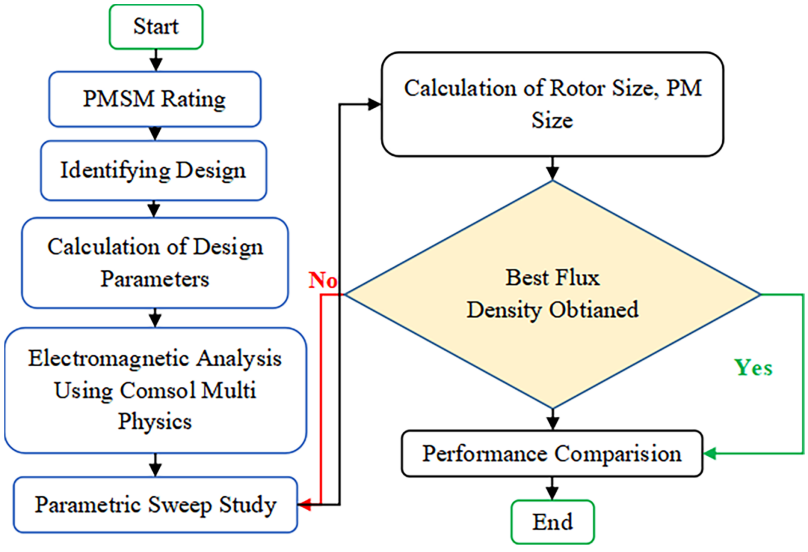

Figure 3: Technical route used to conduct the research

In automotive applications, motor performance is critical. Optimizing the permanent magnet topology is key to enhancing torque characteristics and magnetic flux density in the PMSM, which helps minimize losses. Advanced magnetic materials featuring greater flux density, enhanced permeability, and lower specific iron loss can further minimize iron losses.

The SBW system depicts vehicle steering technology by substituting mechanical linkages with electronic parts, as shown in Fig. 4. The SBW wheel subsystem, such as angle and torque sensors, captures the driver's input and transmits these messages to the steering control unit. This controlling unit is the front wheel steering motor, converting input into accurate wheel movement. Feedback motors offer the driver real road sensations, boosting the driving experience. The integration of these systems enables responsive steering, control, and adaptability, which will lead to future electric and autonomous vehicles, where such technologies are integral to enhanced performance and safety.

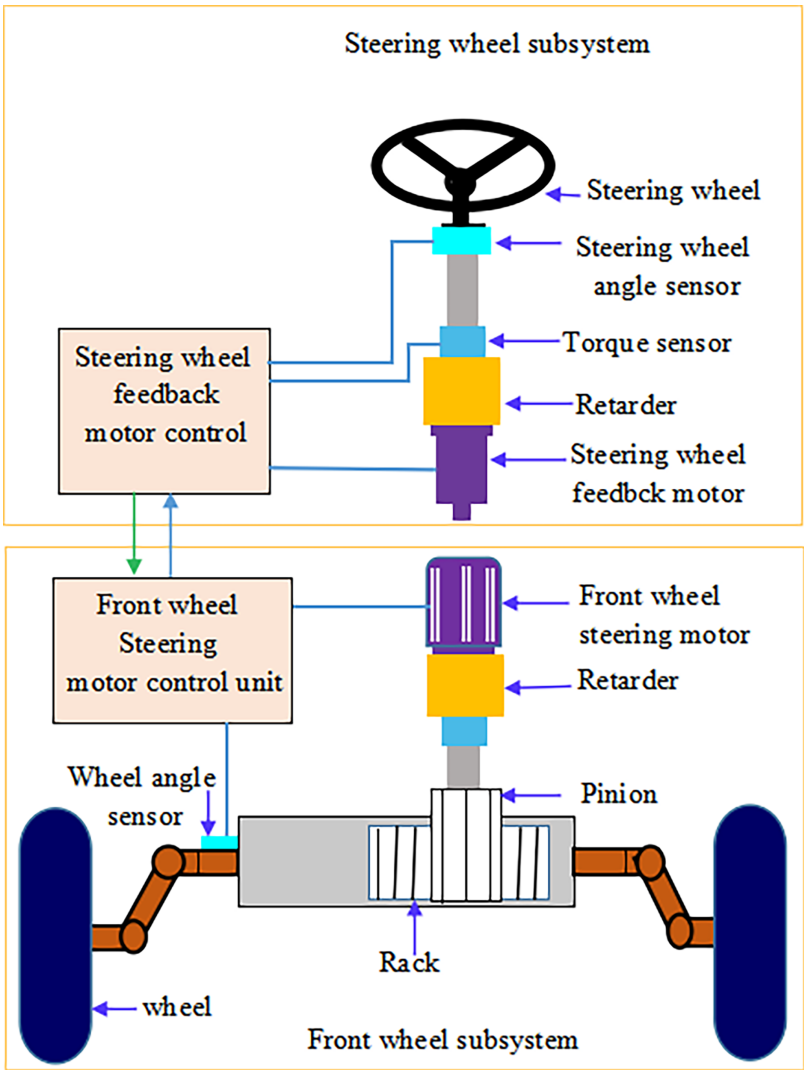

Figure 4: Structure diagram of steer-by-wire

2.1 Force Equations

This section focuses on determining the total force required, given that the designed PMM is intended for use in an electric vehicle application. The main requirement is that the motor must overcome air resistance to propel the vehicle forward [8]. The formula for calculating air resistance is presented below.

$$F_a = C \times S \times \frac{\rho}{2} \times \frac{V_r^{\,2}}{3600} \tag{1}$$

where C stands for the coefficient of air resistance, S indicates the cross-sectional area (m^2), ρ represents the air density (kg/m^3), and V_r denotes the relative velocity of the vehicle in relation to the wind (km/hr). In addition to air resistance, rolling resistance must be considered when calculating the total force requirement and is determined using the following formula.

$$F_r = f_c \times m \times g \times \cos\alpha \tag{2}$$

where f_c is the coefficient of rolling resistance, m is the total mass of the vehicle in kg, g is the gravitation (m/s^2), and α is the slope angle and it can be calculated as follows:

$$F_g = m \times g \times \sin\alpha \tag{3}$$

$$F_m = m \times x \tag{4}$$

2.2 Magnetic Modeling

The operation of a permanent magnet motor, illustrated in Fig. 1b, relies on the efficient transformation of energy from electrical to magnetic and subsequently from magnetic to mechanical energy [11,14]. Consequently, developing precise methods for torque calculation is essential, as the magnetic energy is a critical component of this transition. An important aspect of this process involves determining the distribution of the magnetic field within the motor, as it directly influences the magnetic energy [17,19]. The characteristics of the magnetic field are defined by two fundamental vector quantities: magnetic flux density (B) and magnetic field intensity (H), which are related through the following equation.

$$B = \mu \times H \tag{5}$$

where μ is the permeability of the material.

Magnetic flux refers to the flux density that passes through a designated area. It can be expressed as:

$$\phi = B \times A \tag{6}$$

In this context, A denotes the cross-sectional area of the material. The total variation in magnetic field intensity due to distance is termed magnetomotive force, which is defined as follows:

$$F = H \times L \tag{7}$$

where L is the length, the ratio of ϕ and F give the magnetic permanence, it is defined as:

$$P = \mu \times A/L \tag{8}$$

By using P, reluctance can be found as;

$$R = 1/P \tag{9}$$

After defining the essential equations, the next task is to clarify additional important magnetic relationships. In every PMM design, magnetic flux travels through the air gap that exists between the rotor and stator. Consequently, accurate modeling of the reluctance in this air gap is essential. The reluctance of the air gap can be calculated for various applications using the formula presented as:

$$P_g = (\mu_0) \times \left(A/L_{ge}\right) \tag{10}$$

where L_{ge} is the effective air gap length. It is expressed as;

$$L_{ge} = K_c \times L_g \tag{11}$$

In this context, K_c is Carter's coefficient, while g indicates the length of the air gap. Carter's coefficient serves as a metric to assess the contracted or effective slot pitch for an armature featuring open or semi-enclosed slots. The K_c parameter is defined as follows:

$$K_c = \left[1 - \frac{1}{\frac{\tau_s}{w_s} \times \left(\frac{5 \times L_g}{w_s} + 1\right)}\right] - 1 \tag{12}$$

where τ_s denotes the distance between two magnets and w_s is the distance between two slots.

After establishing the permeance of the air gap, it becomes easy to calculate the reluctance of the air gap. However, the modeling of the air gap's permeance, P_g, is complicated by the fact that flux does not travel directly through the air gap. The resulting fringing effects lead to what is known as fringing permeance, which is expressed as follows:

$$P_f = \left(\frac{\mu_0 \times L_d}{\pi}\right) \times \mathrm{In}\left(1 + \frac{\pi \times x}{L_g}\right) \tag{13}$$

In this case, L represents the depth of the block into the page, while x indicates how far the fringing permeance extends along the sides of the blocks. The expression for magnet permeance is presented as follows:

$$P_m = \mu \times A_m/L_m \tag{14}$$

Here, A_m denotes the cross-sectional area of the magnet, and L_m refers to the thickness of the magnet. The permeance coefficient is calculated using the ratio of the magnet's length to the air gap's length, along with the flux concentration factor, expressed in the following manner:

$$P_c = L_m/L_g \times C_\phi \tag{15}$$

where C_ϕ is the flux concentration factor, defined as:

$$C_\phi = A_m / A_g \tag{16}$$

where A_g is the cross-sectional area of the air gap.

For the magnet to operate safely, the permeance coefficient should exceed one, and the magnet's length ought to be significantly greater than the length of the air gap [1]. Furthermore, increasing the air gap flux density via flux concentration $C_\phi > 1$ leads to a reduction in the permeance coefficient. After formulating the equations, the air gap flux density can be determined as follows:

$$B_g = \frac{K_l \times C_\phi}{1 + \frac{K_r \times \mu_r}{P_c}} \times B_r \tag{17}$$

In this context, K_l represents the leakage factor, K_c is the reluctance factor, and B_r denotes the remanence. For the motor in question, which employs surface-mounted magnets, the leakage factor typically resides within a defined range $0.9 < K_l < 1.0$, the reluctance factor also falls within specific limits $1.0 < K_r < 1.2$, and the ideal value for the flux concentration factor is 1.0. Assuming these values and the remanence are fixed based on the magnet chosen, the amplitude of the air gap flux density is governed by the permeance coefficient P_c. As the permeance coefficient increases, the air gap flux density B_g approaches a maximum value that is just below B_r, the remanence.

2.3 Coil Resistance and Coil Inductance

Motors typically employ multiple interconnected coils to create distinct phases. These coils inherently possess resistance and inductance. Accurately modeling inductance, particularly when mutual inductance effects are significant, presents a considerable challenge. In general, the resistivity of a material depends on temperature, and the relationship between resistivity and temperature is frequently represented as an exponential function, as illustrated below.

$$\rho\,(T) = \rho\,(T_0) \times [1 + \alpha_t \times (T - T_0)] \tag{18}$$

In this context, T denotes the temperature, T_0 refers to the reference temperature, and α_t is the thermal resistivity coefficient. The use of slots in motor design is essential for achieving the correct alignment of the coils. Consequently, accurate slot calculations are a necessary component of the design process. To determine the slot resistance, it is first necessary to define the slot fill factor. The wire slot fill factor is defined as follows.

$$K_{wb} = N \times A_{wb}/A_s \tag{19}$$

In this case, N stands for the number of turns, A_s indicates the cross-sectional area of the slot, and A_{wb} refers to the cross-sectional area of the bare wire and can be represented as:

$$A_{wb} = W_{th}/d_s \tag{20}$$

where, L_t denotes the tooth length, and w_s represents the width of the slot. Once the slot fill factor has been determined, the slot resistance R_s can be calculated.

$$R_s = \left(\rho\,(T) \times L \times N^2\right)/(K_{wb} \times A_s) \tag{21}$$

Inductance might not be the primary factor in every PMM design, it plays a crucial role in establishing the time constant of the winding, which in turn affects the rate at which winding currents change. Coils have both self-inductance and mutual inductance. Self-inductance is the effect of one coil on another coil in the same phase, while mutual inductance is the effect of one coil on another coil in a different phase. However, this analysis focuses on the mutual inductance between coils within the same phase, since the mutual inductance between different phases is typically much less than self-inductance. When coils are put in slots, their inductance has three parts, each of which corresponds to an area where the current in the coils creates a strong magnetic field. These areas encompass the air gap, the slots, and the end turns, as described below.

$$L_g = \frac{2\pi \times \mu_o \times l \times R_{ro}}{1 + \frac{i}{\mu_r \times C_\phi}} \times N_c^{\,2}$$

$$L_s = N_m \times (2 \times N_c)^2 \times \left[\frac{\mu_o \times d_s \times L}{3 \times w_{sb}} + \frac{\mu_o \times d_t \times L}{\frac{w_{so} + w_{sb}}{2}} + \frac{\mu_0 \times d_{sh} \times L}{w_{so}} \right] \tag{22}$$

$$L_e = \frac{N_m \times \mu_o \times \tau_{cp} \times N^2}{2} \times 1n\left(\frac{\tau_{cp} \times \sqrt{\pi}}{\sqrt{2 \times A_s}}\right)$$

In this context, N_c refers to the number of conductors, N_m indicates the number of magnets, l represents the length of the motor, r_g is the radius of the air gap, d_t is the distance from the tooth to the entrance, t_e denotes the thickness of the slot entrance, w_s is the width of the slot, and w_e indicates the width of the slot entrance.

2.4 Electromagnetic Force and Torque Analysis

In a PMSM, the electromotive force (EMF) arises from the interaction between the permanent magnets on the rotor and the windings of the stator, playing a vital role in torque generation. The strength of the back EMF depends on the speed of the rotor, the density of the magnetic flux, and the number of turns present in the stator winding [20–23].

$$E = k \times \phi \times N \times \omega \tag{23}$$

where, E: back EMF, k: constant related to motor design, ϕ: magnetic flux, N: number of turns in the winding, ω: angular velocity of the rotor.

The EMF waveform shows harmonic distortion due to variations in rotor geometry and stator winding configurations, affecting motor performance and torque characteristics [6]. Torque production in PMSM involves two main components: the permanent magnet torque and the reluctance torque. The total electromagnetic torque (T_e) can be expressed as:

$$T_e = T_{pm} + T_r T_e = T_{pm} + T_r \tag{24}$$

where T_{pm} is torque produced by permanent magnets, T_r is reluctance torque.

3 Finite Element Analysis

The design of a permanent magnet synchronous motor (PMSM) has four key stages. In the first stage, we defined the key geometric parameters that impact torque, efficiency, and overall motor behavior. The stator design focuses on the best winding configurations and material selection to reduce losses. The rotor is designed to include permanent magnets, carefully positioned for maximum electromagnetic interaction with the stator. Lastly, performance estimation includes simulating operational characteristics to assess efficiency and torque. The new model is based on the values in Table 1, and Fig. 5a,b show the finer mesh for both 2D and 3D simulations. The time complexity of the FEA is a crucial consideration in our analysis, as it mainly affects both the precision of the simulation results and the computational resources required. FEM solves systems of partial differential equations, and as we increase the mesh refinement to capture complex electromagnetic interactions more accurately, the number of elements rises. This results in exponential growth in computational time and memory usage, which needs to be carefully managed to maintain feasibility.

Table 1: Design parameters of new PMSM model [2]

Components	Value
Outer radius of the stator (mm)	45
Inner radius of the stator (mm)	24
Stator back iron depth (mm)	5
Stator tooth width (mm)	4
Number of phases	3
Stator pole (pairs)	6
Stator slots	12
Air gap (mm)	1
Stator and rotor core	M19-29G
Permanent magnet material	NdFeB (N50)
Shaft	Iron
Winding	Copper

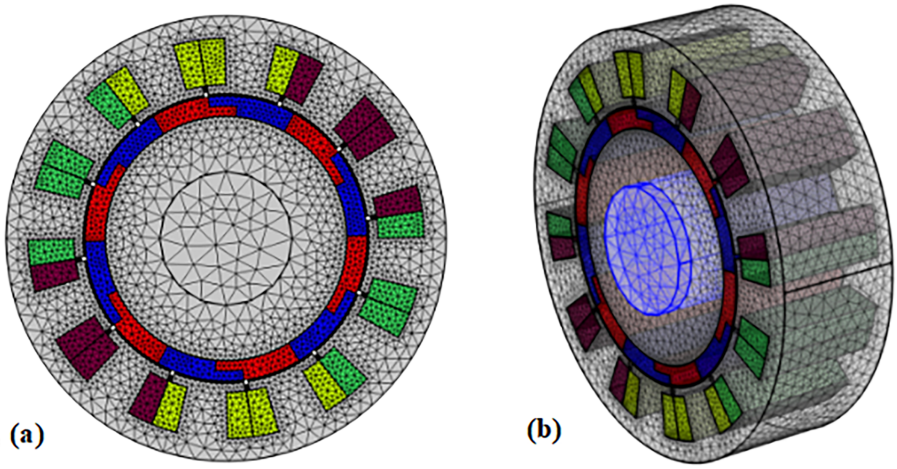

Figure 5: The corresponding mesh for (a) 2D and (b) 3D of the model, respectively

Flux Density

Magnetic flux density in PMSM can be analyzed using 2D and 3D models. 2D models in Fig. 6a indicate a flux density of 3.2 T and are useful for the initial design stage, but they oversimplify the magnetic field by neglecting end effects. The 3D models, as shown in Fig. 6b with a density of 3.66 T, provide a more precise depiction, including complex geometries and spatial variations.

The remanent flux density of permanent magnets is crucial for the functioning of PMSM. In two-dimensional models, a remanent flux density of 2.05 T is illustrated in Fig. 7a; however, this value may be inflated due to the exclusion of end effects. Conversely, the three-dimensional model results presented in Fig. 7b reflect a remanent flux density of 2.19 T, offering a more accurate depiction of the motor's intricate magnetic field dynamics.

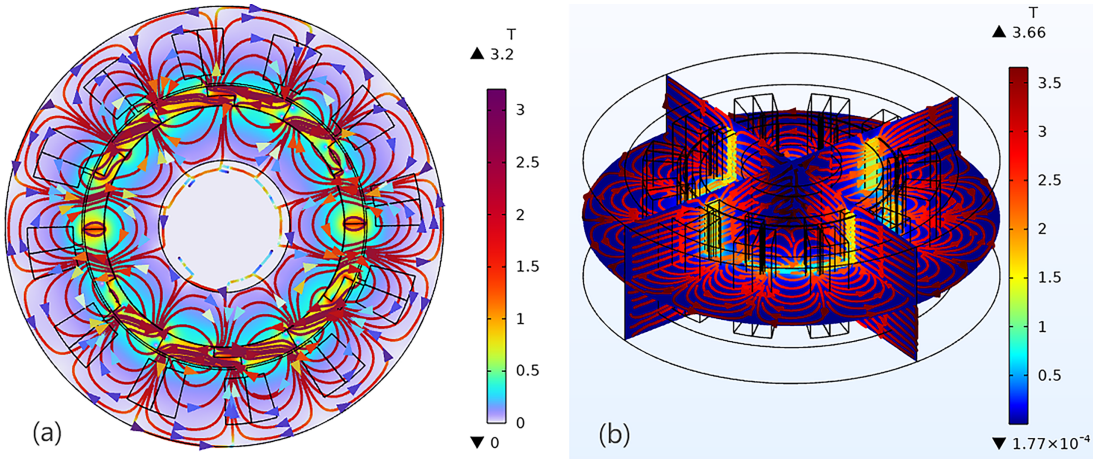

Figure 6: (a) 2D and (b) 3D, PMSM model flux density

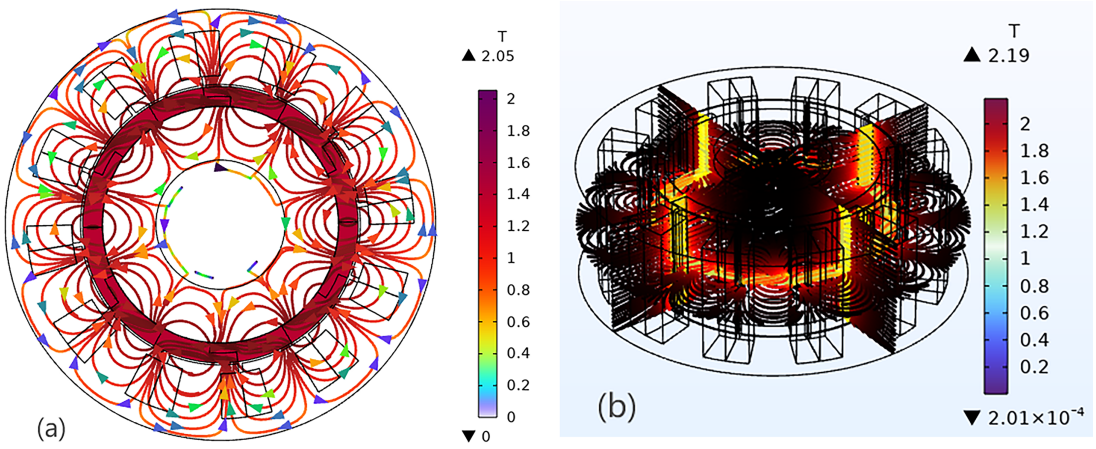

Figure 7: (a) 2D and (b) 3D PMSM model remanent flux

4 Result and Discussion

This section evaluates the effectiveness of the newly proposed design for the permanent magnet synchronous motor. It presents key characteristics, including phase current, voltage, power, and winding coil flux. Additionally, the results are validated through a comparative analysis with conventional PMSM designs, focusing on magnetic torque, flux density, and torque ripple. This comparison offers information about the improvements achieved by the new design.

Figs. 8 and 9 show phase current and voltage in PMSM, both critical for motor performance. The number of winding turns affects phase current, necessitating an optimal value to avoid excess current and ensure overload capacity. Accurate current measurement is crucial to prevent torque pulsations. Phase voltage, influenced by winding configuration and inverter voltage levels, impacts the required DC voltage and includes voltage harmonics.

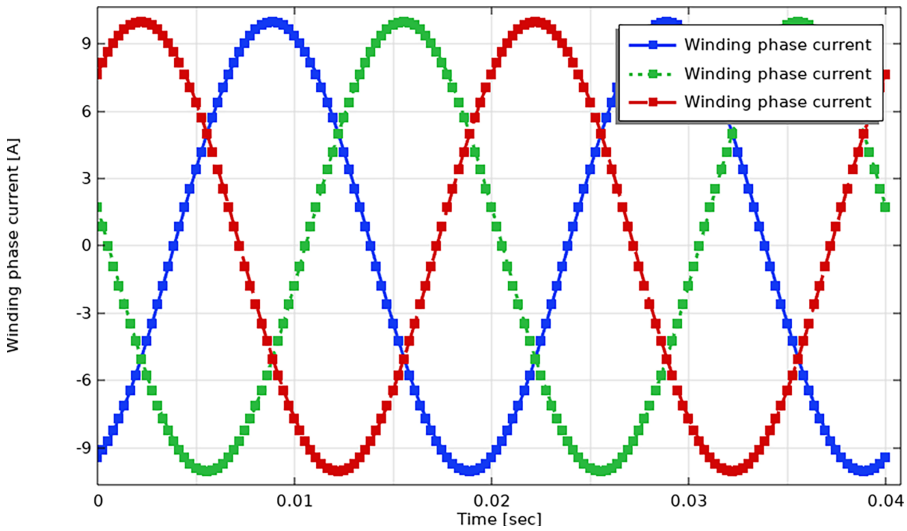

Figure 8: Phase current on the winding coils of PMSM model

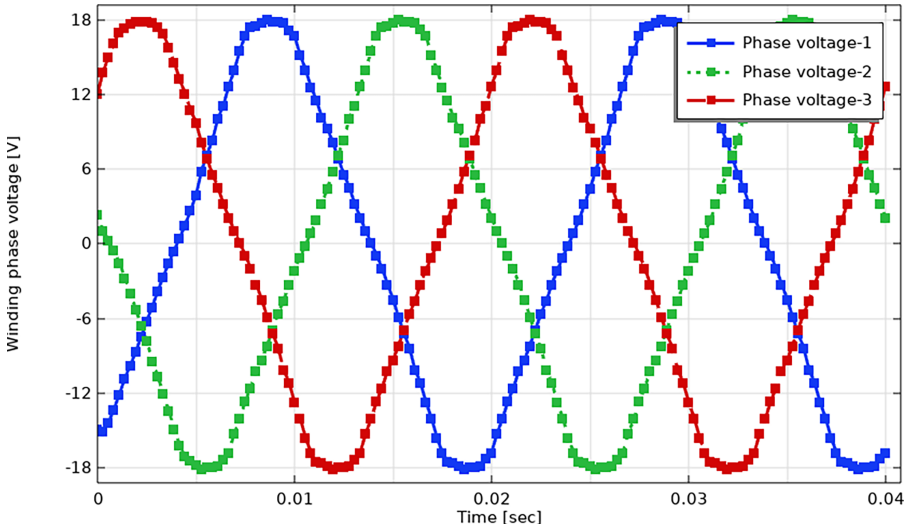

Figure 9: Phase voltage of PMSM model

Fig. 10 depicts that phase power in PMSM is impacted by winding turns, current, and voltage. Fractional slot winding improves power density, while distributed winding promotes a near-unity power factor. Fig. 11 illustrates that phase flux, generated by rotor magnets, is crucial for torque and based on winding turns and material selection.

The air gap thickness in a PMSM plays a key role in determining the magnetic torque produced by the new proposed motor. A rise in air gap thickness leads to higher magnetic reluctance, which in turn reduces the magnetic flux density within the air gap. This reduction in flux density affects the torque output, as the torque in a PMSM arises from the interaction between the magnetic field of the stator and the rotor's PMs; see Fig. 12.

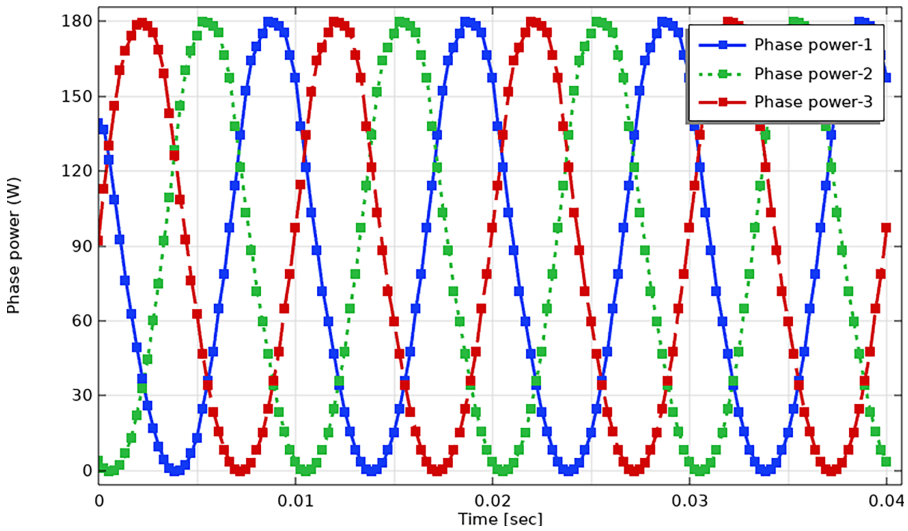

Figure 10: Phase power of proposed PMSM model

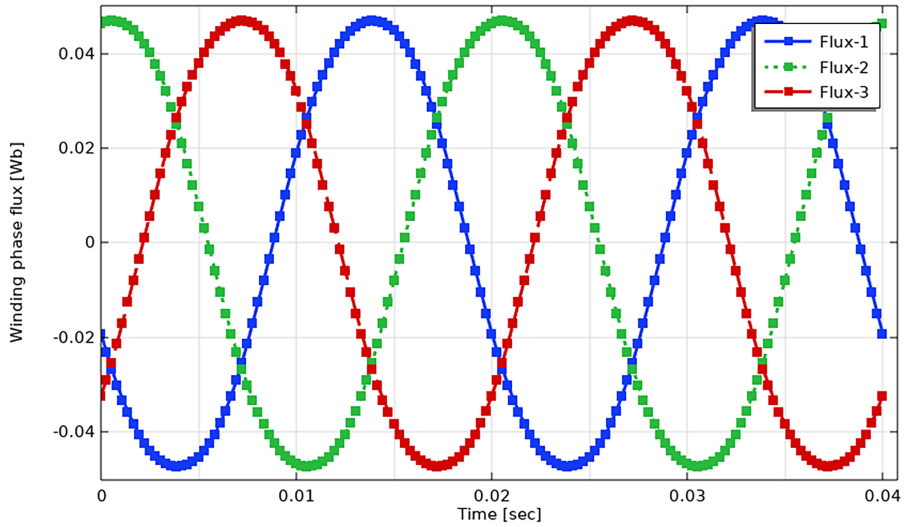

Figure 11: Phase flux plot of proposed PMSM model

The thickness of permanent magnets in a PMSM impacts the magnetic flux density within the motor. Typically, a thicker magnet provides more magnetic material for flux generation, resulting in higher magnetic flux density in both the air gap and rotor. This increased flux density enhances torque production, as a stronger magnetic field interacts more efficiently with the armature current; see Fig. 13.

Model Validation

This section presents the validation of the model by comparing the new PMSM model with the existing design. The analysis was performed using MATLAB 2021 and assessed magnetic flux density, torque, and torque ripple.

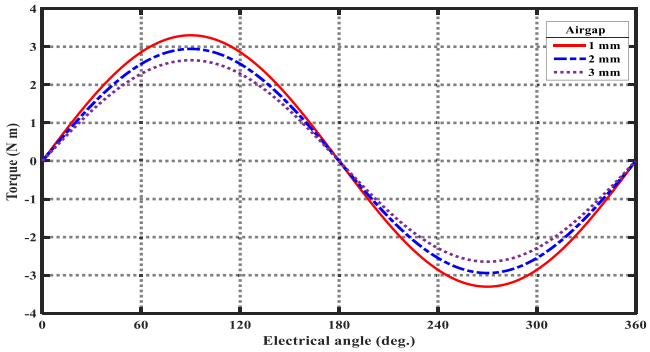

Figure 12: Impact of air gap on torque performance

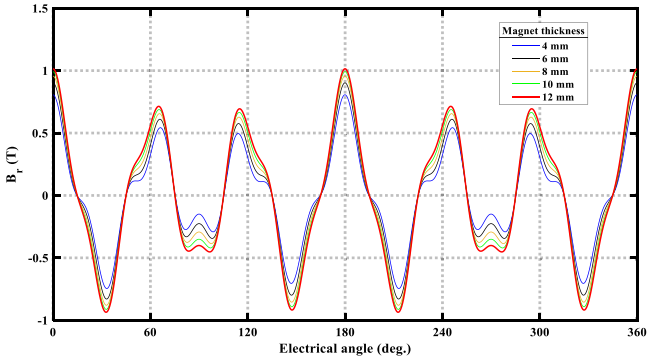

Figure 13: Impact of PM thickness on flux density of PMSM

Fig. 14 shows that the proposed PMSM design has a higher magnetic flux density. This offers better performance. Fig. 15 show an increase in magnetic torque of 4.65%, due to the new PM topology, high-performance magnetic materials, and good rotor structures. Additionally, Fig. 16 depicts the newly designed PMSM reducing torque ripple by 4.4%, further boosting performance.

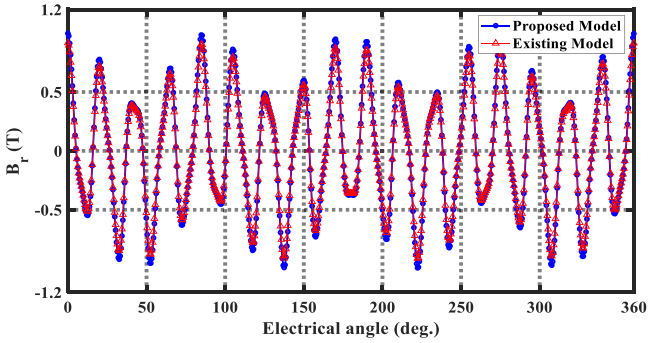

Figure 14: Flux density comparison

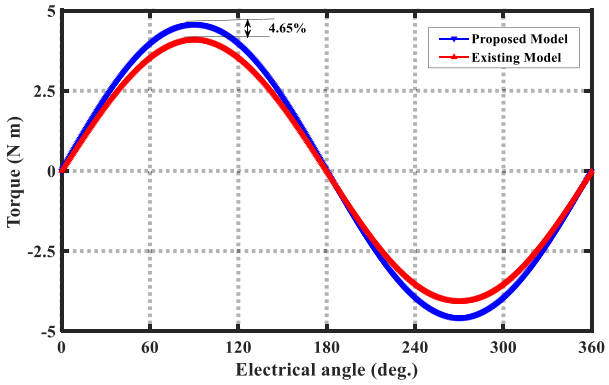

Figure 15: Static torque vs. rotor angle plot

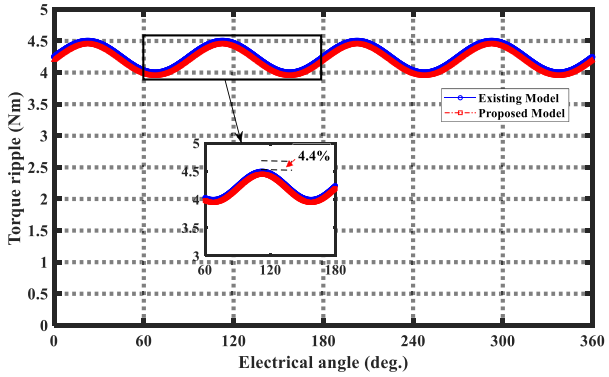

Figure 16: Torque ripple plot

5 Conclusion

Improving the performance of permanent magnet synchronous motors (PMSM) presents ongoing challenges for motor designers in vehicle steering systems. Boosting performance while minimizing weight is essential for overall improvements in steering systems. One technique to overcome these issues is the implementation of a new PM topology, which can replace conventional designs to reduce losses, weight, and size in PMSMs. Additionally, the new rotor shape of the L-shaped PMSM can increase static torque performance by 4.65%. These PMSM designs contribute to safer, more comfortable driving experiences and support the development of intelligent automotive technologies in vehicle steering systems.

Furthermore, considerations regarding manufacturability and cost are critical. The new L-shaped model facilitates cost reductions by lowering material usage, simplifying manufacturing processes, and reducing energy losses. These factors not only lower manufacturing costs but also improve the motor's performance-to-cost ratio, making it a compelling choice for modern vehicles. However, future research should explore the scalability of the new topology to different motor sizes and configurations, as well as assess the long-term reliability of the L-shaped rotor in various operating conditions. This will provide clear insights into the various applications of PMSM's next-generation automotive designs.

Acknowledgement: Not applicable.

Funding Statement: The authors received no specific funding for this study.

Author Contributions: Mahmud Ebrahim Assen developed the modeling framework for the novel permanent magnet motor and conducted simulations to assess its impact on vehicle steering performance. Guoqing Geng supervised and analyzed the simulation results, validating the motor design. All authors reviewed the results and approved the final version of the manuscript.

Availability of Data and Materials: The datasets generated and/or analyzed during the current study are available from the corresponding author on reasonable request.

Ethics Approval: Not applicable.

Conflicts of Interest: The authors declare no conflicts of interest to report regarding the present study.

References

1. Patel A, Jhankal T. Performance enhancement of high speed interior permanent magnet synchronous motors using superior magnetic material. Trans Energy Syst Eng Appl. 2023;4(1):18–34. doi:10.32397/tesea.vol4.n1.505.
2. Proca AB, Keyhani A, El-Antably A, Lu W, Dai M. Analytical model for permanent magnet motors with surface mounted magnets. IEEE Trans Energy Convers. 2003;18(3):386–91. doi:10.1109/TEC.2003.815829.
3. Rsetam K, Zheng Y, Cao Z, Man Z. Adaptive active disturbance rejection control for vehicle steer-by-wire under communication time delays. Appl Syst Innov. 2024;7(2):22. doi:10.3390/asi7020022.
4. Mortazavizadeh SA, Ghaderi A, Ebrahimi M, Hajian M. Recent developments in the vehicle steer-by-wire system. IEEE Trans Transp Electrif. 2020;6(3):1226–35. doi:10.1109/tte.2020.3004694.
5. Wilwert C, Navet N, Song YQ, Simonot-Lion F. Design of automotive X-by-wire systems. In: Zurawski R, editor. The industrial communication technology handbook. Boca Raton, FL, USA: CRC Press; 2005. p. 0849330777.
6. Pei W, Zhang Q, Li Y. Efficiency optimization strategy of permanent magnet synchronous motor for electric vehicles based on energy balance. Symmetry. 2022;14(1):164. doi:10.3390/sym14010164.
7. Choi G, Jang GH, Choi M, Kang J, Kang YG, Kim S. Optimal design of a surface permanent magnet machine for electric power steering systems in electric vehicle applications using a Gaussian process-based approach. Actuators. 2024;13(1):13. doi:10.3390/act13010013.
8. Kim HJ, Baek SW. Optimal shape design to improve torque characteristics of interior permanent magnet synchronous motor for small electric vehicles. Microsyst Technol. 2025;31(5):1203–17. doi:10.1007/s00542-024-05699-8.
9. Xia Y, Lv S, Jing B, Zhou Z. Improvement of heat dissipation structure of low speed permanent-magnet motor. IEEE Access. 2023;11:51789–97. doi:10.1109/access.2023.3278276.
10. Deepak K, Frikha MA, Benômar Y, El Baghdadi M, Hegazy O. In-wheel motor drive systems for electric vehicles: state of the art, challenges, and future trends. Energies. 2023;16(7):3121. doi:10.3390/en16073121.
11. Qi Z, Zhang Y. Comparative study of a high-speed permanent magnet motor when powered by different methods. IET Electr Power Appl. 2024;18(8):924–40. doi:10.1049/elp2.12449.
12. Zhu Z, Chai X, Xu L, Quan L, Yuan C, Tian S. Design and performance of a distributed electric drive system for a series hybrid electric combine harvester. Biosyst Eng. 2023;236(2):160–74. doi:10.1016/j.biosystemseng.2023.10.015.

13. Guo L, Wang Y, Wang H, Zhang Z. Design of high power density double-stator permanent magnet synchronous motor. IET Electr Power Appl. 2023;17(4):421–31. doi:10.1049/elp2.12275.
14. Wang X, Liu S, Wang L, Gao P. Impact of the motor length-to-diameter ratio on the selection of cooling water channels for the PMSM. IEEJ Trans Electr Electron Eng. 2023;18(11):1815–25. doi:10.1002/tee.23905.
15. Li Z, Wang P, Liu L, Xu Q, Che S, Zhang L, et al. Loss calculation and thermal analysis of ultra-high speed permanent magnet motor. Heliyon. 2022;8(11):e11350. doi:10.1016/j.heliyon.2022.e11350.
16. Ge B, Wang Y, Xu X, Wang L, Huang S, Yang Z. Research on loss differences and thermal optimisation of submerged cryogenic high-speed permanent magnet motors. IET Electr Power Appl. 2024;18(11):1554–66. doi:10.1049/elp2.12492.
17. Li J, Wu Z, Li M, Shang Z. Dynamic measurement method for steering wheel angle of autonomous agricultural vehicles. Agriculture. 2024;14(9):1602. doi:10.3390/agriculture14091602.
18. Sahoo AK, Chakraverty S. Machine intelligence in dynamical systems: \a state-of-art review. WIREs Data Min Knowl. 2022;12(4):e1461. doi:10.1002/widm.1461.
19. Zhang J, Zhang J, Liu Z. Numerical evaluation of the heat transfer performance of water-cooled system for electric vehicle drive motor based on the field synergy principle. Therm Sci. 2024;28(2 Part A):823–35. doi:10.2298/tsci230422164z.
20. Ravanbod M, Montazeri A. A novel auxetic stator winding to improve the performance of permanent magnet synchronous electric motors. Eng Res Express. 2024;6(1):015095. doi:10.1088/2631-8695/ad3148.
21. Yu Y, Hao S, Guo S, Tang Z, Chen S. Motor torque distribution strategy for different tillage modes of agricultural electric tractors. Agriculture. 2022;12(9):1373. doi:10.3390/agriculture12091373.
22. Soresini F, Barri D, Ballo F, Gobbi M, Mastinu G. Noise and vibration modeling of permanent magnet synchronous motors: a review. IEEE Trans Transp Electrif. 2024;10(4):8728–45. doi:10.1109/tte.2024.3365151.
23. Aslan M, Özpolat AB, İşçi C, Eroğlu F, Vural AM. Design and modelling of internal permanent magnet motor. Int J Energy Eng Sci. 2020;5(2):80–104.